Asian Journal of Physics Vol. 5, No. 2 (1996) 87-110

Continuum resonance Raman scattering in $^{79}Br^{35}Cl$

M SCHMITT, P VOGT AND W KIEFER*

Institut für Physikalische Chemie der Universität Würzburg
Marcusstrasse 9-11, D-97070 Würzburg, Federal Republic of Germany

High resolution continuum resonance Raman spectra of isotopically pure $^{79}Br^{35}Cl$ were recorded with excitation by several argon ion laser lines from the visible to the UV region. With excitation in the UV region spectra also of higher overtones could be observed. The cŏmplex rovibrational structures are explained in terms of Q branches, unresolved S bands and S band heads, unresolved O branches and corresponding hot band transitions. The experimentally observed spectra were simulated using both the conventional and time-dependent quantum theory. The simulations of the observed spectra together with results from depolarization ratio measurements allowed us to discuss the excited state potential functions involved in this type of resonance Raman scattering. The high sensitivity of resonance Raman band shapes to changes in the position of excited potential curves gives the possibility of determining the potential functions of the excited states $^1\Pi_1$ and $^3\Pi_{0+}$. The spectral features of the fundamental Raman band could be explained assuming nonresonant Raman scattering resulting from adjacent highly lying states.

1 Indroduction

The Raman spectra of the fundamental region in gaseous BrCl was first observed by Stammreich and Forneris[1] already in 1953. The Raman spectra of liquid BrCl [Ref. 2] and BrCl isolated in cold argon matrix[3] were also reported.

Continuum resonance Raman scattering of gaseous bromine chloride was first studied by Holzer, Murphy and Bernstein[4] in 1970. In this work they investigated many halogen and interhalogen gases such as Cl_2, Br_2, I_2, BrCl, ICl and IBr as examples to study the phenomena and characteristics of continuum resonance Raman scattering versus resonance fluorescence. These authors could observe the resonance Raman spectra of the fundamental and the first overtone of BrCl in a mixture of natural Br_2 and Cl_2, where a certain amount of BrCl was

* Author to whom correspondence should be addressed

formed from the chemical equilibrium reaction of Cl_2 with Br_2. As exciting laser lines only the visible lines of an argon ion laser were used. The interhalogen molecules ICl, IBr and BrCl have also been the subject of extensive studies by Chang and co-workers[5-7]. They obtained the continuum resonance Raman spectra of natural BrCl with excitation in the visible region. The resolutions of the reported spectra were about 1 cm^{-1} for the fundamental region and more than 3 cm^{-1} for the overtones.

Holzer *et al*[4] as well as Chang *et al*[5-7] observed a very high intensity of the fundamental ($\Delta v=1$) Raman band when compared to the intensity of the overtones. Strempel and Kiefer[8] observed a similar phenomenon for $^{35}Cl_2$. They explained this high intensity of the fundamental region assuming nonresonant Raman scattering resulting from adjacent highly lying states. Their results were based on the observed depolarization ratios of the fundamental transitions, the changes in relative intensities between the different Q branches of the fundamental bands and comparison of the observed and calculated overall band intensities of the fundamental and overtone bands excited with different laser lines.

Most of the halogen and interhalogen molecules have different isotopic species, which complicate the theoretical simulation of the experimental spectra. In addition the spectra of the molecules in their natural abundance cannot be resolved in their rotational-vibrational fine structure as much as it would be possible for the single isotopic species. In order to obtain accurate information on the excited state repulsive potential functions for the interhalogen molecules also a comprehensive experimental study of continuum resonance Raman scattering in isotopically pure $^{127}I^{79}Br$ [Ref. 9] and $^{127}I^{35}Cl$ [Ref. 10] has been performed in our laboratory.

Experimentally observed continuum resonance Raman spectra of halogen molecules have been traditionally simulated by applying the Kramers-Heisenberg-Dirac (KHD) relationship[11,12], which contains only time independent quantities. Such calculations were first performed on iodine by Rousseau and Williams[13]. Baierl and Kiefer[14-16] simulated the spectra of isotopically pure bromine and achieved good results for the fundamental vibrational transition. For the same molecule interference effects between two contributing electronic states could be observed[17]. Comprehensive new numerical calculations using the traditional KHD-relationship has been performed for isotopically pure $^{35}Cl_2$ [Ref. 8], $^{79}Br_2$ [Ref. 18], $^{127}I_2$ [Ref. 19], $^{127}I^{35}Cl$ [Ref. 20,21] and for $^{127}I^{79}Br$ [Ref. 22].

During the past decade an alternative time-dependent theory has been pioneered by Hizhnyakov and Tehver[23], Heller *et al*[24-26], Williams and Imre[27] and

others[28]. This approach has been succsessfully applied to continuum resonance Raman scattering in $^{79}Br_2$ by Hartke[29-31], who showed equivalent results obtained by both the time-independent and time-dependent approaches. Works related to this were performed in isotopically pure $^{127}I_2$ [Ref. 32] and $^{127}I^{35}Cl$ by Ganz *et al*[20] and Ganz and Kiefer[21] and in $^{127}I^{79}Br$ by Vogt and Kiefer[22] and Ganz and Kiefer[32]. Results on $^{35}Cl_2$ concerning the time dependent theory and spectra with excitation in the deep UV region were recently obtained[34].

Similar detailed investigations for the BrCl molecule particulary for the isotopically pure $^{79}Br^{35}Cl$ molecule are still missing. In this paper we present experimental and theoretical work on this molecule and report on continuum resonance Raman spectra of $\Delta v=1$ to $\Delta v=6$ transitions excited over a wide range of excitation from the visible to the UV region. Advanced spectroscopic techniques which include CCD detection and the scanning multi-channel techniques (SMT)[35] were applied for these studies in order to obtain high resolution spectra, which are then simulated applying both theoretical approches as mentioned above.

2 Theory and numerical calculation

The time-dependent and time-independent theory for the calculation of continuum resonance Raman spectra have been described earlier in detail (see e.g. Ref. [21] and References cited therein). Expressions for continuum resonance Raman intensities were derived in these papers which allow a numerical calculation of single vibrational transition when resonance with continuous electronic states takes place.

For the numerical simulation of the observed continuum resonance Raman spectra of $^{79}Br^{35}Cl$ we first need the relevant potential functions as outlined in chapter 3 of Ref. [21].

The ground state $^1\Sigma^+$ potential function of $^{79}Br^{35}Cl$ is known with high accuracy. The RKR (Rydberg-Klein-Rees method[36-38]) values are taken from Coxon[39] and Mc Feeters *et al*[40]. Between the turning points an interpolation was carried out. The spectroscopic parameters of the ground state have been taken from Ref. [39]. From these data the line positions of the rovibronic transitions are calculated using the standard expressions for the anharmonic oscillator-rigid rotator model with vibration-rotation interaction.

The potential function for the bound region of the $B(^3\Pi_{0^+})$ state was derived from RKR values of Ref. [39]. The repulsive branch of the $B(^3\Pi_{0^+})$ state was

calculated using an exponential expression of the same form as given in Eq. (10) of Ref. [21]. For the purely repulsive state $\Pi(^1\Pi_1)$ state we also used the same exponential form.

Due to the high spectroscopic temperature in the sample cell it was necessary to regard a large number of populated vibrational-rotational levels in the electronic ground state. For $^{79}Br^{35}Cl$ we took into account 6 vibronic levels and 400 rotational levels. For a complete Raman band with O-, Q- and S-branches we therefore considered a total of 7200 rovibronic transitions. The calculated line spectrum for these transitions was then convoluted similarly as for $^{127}I^{35}Cl$ [Ref. 21].

Also the optimization of the potential parameters as well as the final numerical simulation of the observed spectra were performed as described in Ref. [21].

3 Experimental

In order to prepare the isotopically pure $^{79}Br^{35}Cl$ we filled $^{79}Br_2$ and an excess (30%) of $^{35}Cl_2$ in the sample cell. Both isotopically pure halogens were poduced by oxidation of the sodium salts ($Na^{35}Cl$, $Na^{79}Br$: Oak Ridge National Laboratory, purities: 99.35 and 99.41% respectively) with $K_2S_2O_8$. For this kind of oxidation the overall yields were 80 and 98%, respectively. The Raman spectra were recorded with a conventional 90°-scattering arrangement using a Spectra Physics model 2085 Beam Lok™ argon ion laser. In the visible region the laser power was set to 1.5 W for all laser lines except for 465.8 and 454.5 nm (0.9 W). In the UV region the laser power for the two lines at 363.8 and 351.1 nm was 1.5 W each and for the three lines at 335.8, 334.5 and 333.5 nm 0.7 W each. The laser light was focused with an f=40 mm quartz lens into the cell containing $^{79}Br^{35}Cl$. The bromine chloride cell was heated to about 70°C. For this temperature the vapor pressure of the BrCl is about 180 Torr[41]. The scattered light was collected with an f=50 mm (1:0.7) photo objective (for excitation with $\lambda_{exc.} \gtrapprox 400$ nm) or an f=50 mm (1:1.3) quartz lens for excitation below 400 nm and analyzed with a Spex 1404 double monochromator (gratings 2400 lines/mm). The spectral resolution applied in these studies was between 0.6 and 1.5 cm^{-1}. The dispersed Raman stray light was detected with a Photometrics model RDS 200 CCD Raman detection system using the scanning multichannel (SMT) technique[35]. All spectra shown in this paper are original data without application of any smoothing routines.

The temperature in the laser focus is high when excitation is performed in strong absorption regions. The spectroscopic temperature for each laser line was determined via the maximum of pure rotational Raman spectrum[9]. We determined T=680 K for the laser lines in the visible region, except for 465.8 and 454.5 nm (630K), T=850 K for 363.8 and 351.1 nm and T=600 K for 335.8, 334.5 and 333.6 nm. The accuracy is about ±50 K in each case.

4 Results and Discussion

4.1 Survey spectrum

Fig. 1 shows the survey spectrum of $^{79}Br^{35}Cl$ for 363.8 nm excitation and a spectral slit width of 1.5 cm^{-1}. For this wavelength both the bromine chloride and the chlorine give rise to continuum resonance Raman scattering with high overtone progressions as indicated.

In the case of $^{35}Cl_2$ we observed a very strong fundamental band when compared to the intensity of the overtones. This result agrees with the one obtained for pure $^{35}Cl_2$ [Ref. 8] and will be discussed in more detail below.

In order to avoid also strong superposition by $^{79}Br_2$ transitions we have shifted the chemical equilibrium of the reaction $^{79}Br_2 + {}^{35}Cl_2 \rightleftharpoons 2\ {}^{79}Br^{35}Cl$ using a chlorine excess of 30%. The remaining amount of $^{79}Br_2$ is very small and only a very weak overtone progression up to the second overtone can be observed in the survey spectrum (see Fig. 1).

We observed a high number of overtones in $^{79}Br^{35}Cl$ only for the 351.1 and 363.8 nm laser lines. With excitation in the visible region (507.1 - 454.5 nm) the fundamental and only the first overtone could be detected with high resolution (0.5 - 1 cm^{-1}). When excitation with the weak laser lines at 335.8, 334.5, and 333.6 nm is applied then the fundamental, first as well as the second overtone could be observed with high resolution.

Fig. 2 shows the continuous absorption spectra of bromine chloride (panel A) and of the parent molecules bromine (panel B) and chlorine (panel C). These absorption spectra were constructed using data points reported by Seery and Britton[42]. The argon ion laser lines used for excitation in this study are marked by labeled circles in panel A.

As has been observed in many studies, in continuum resonance Raman scattering high overtone progressions can only be observed when excitation is

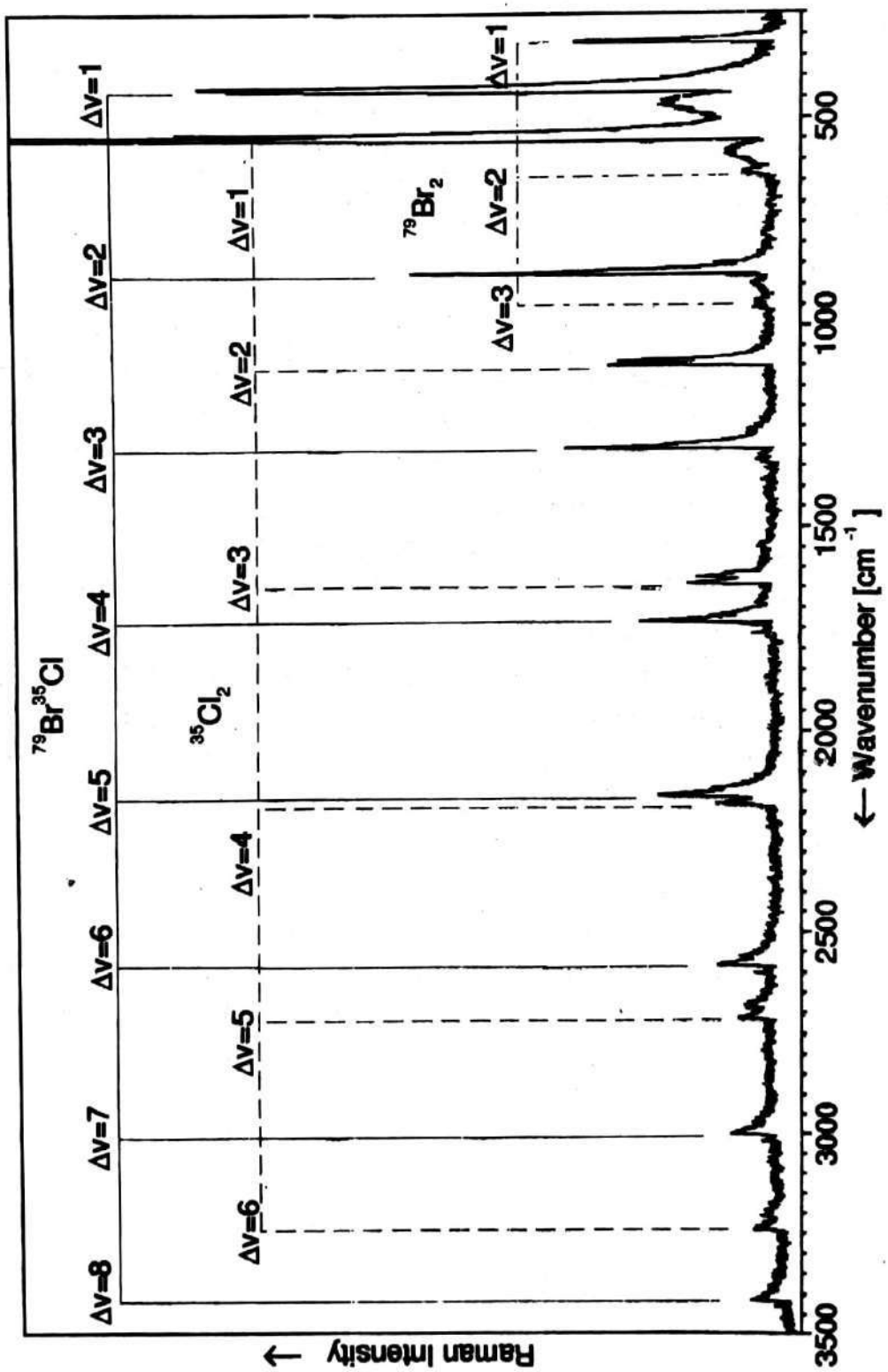

Fig. 1. Survey continuum resonance Raman spectrum of $^{79}Br^{35}Cl$ excited with λ_0=363.8 nm ; slit width s=1.5 cm^{-1} ; laser power P=1.5 W.

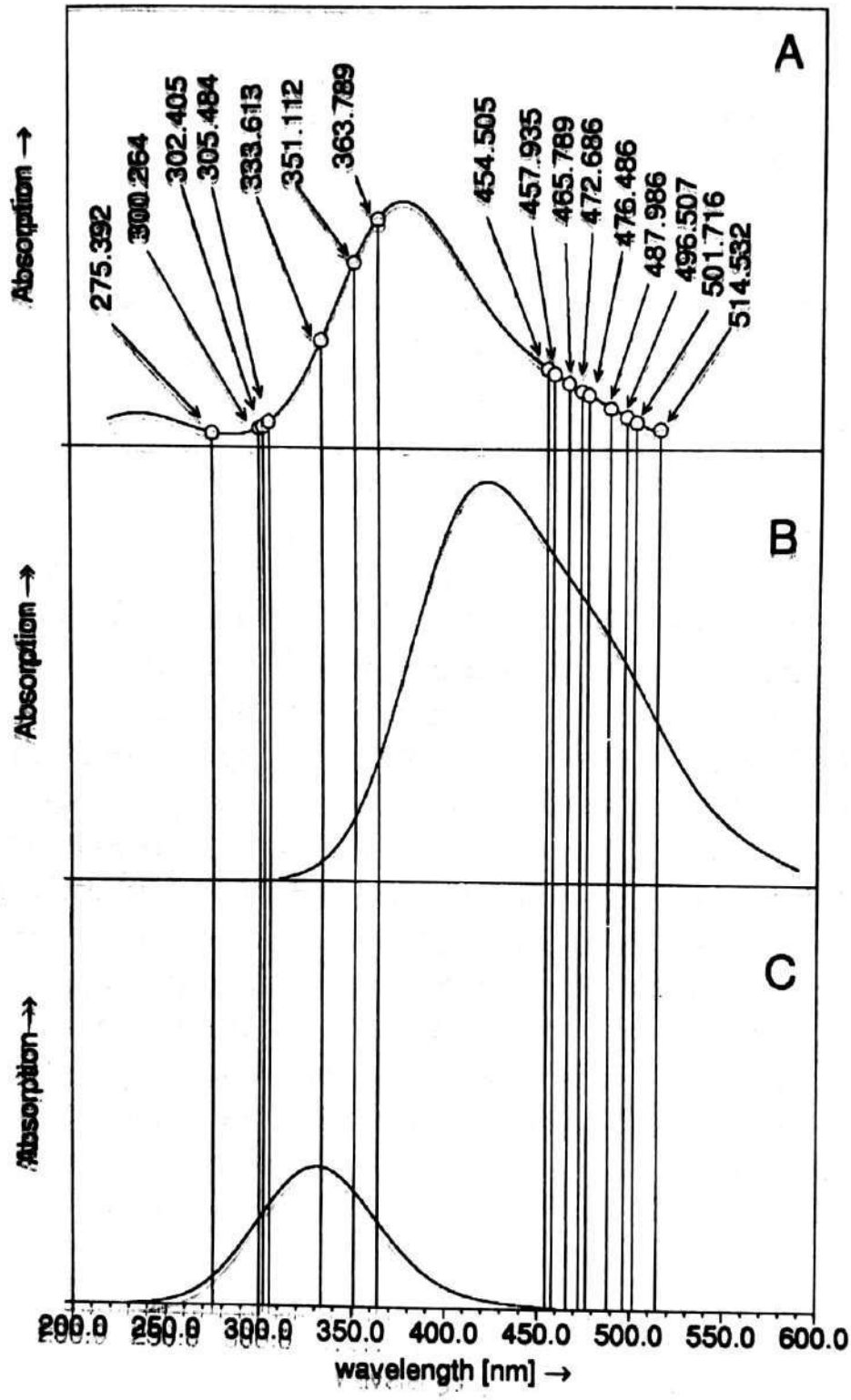

Fig. 2. Continuous absorption spectra of bromine chloride (panel A), bromine (panel B) and chlorine (panel C). Data from Ref. [42] were used for the construction of the spectra. The argon ion laser lines employed in this study are marked by circles and vertical lines.

performed in strong absorption regions. A simple illustrative explanation for this phenomen is given in Ref. 43 applying a time dependent description. For BrCl this condition is only fullfilled for 351.1 and 363.8 nm excitation. In the visible region and in the deeper UV region the BrCl molecule shows lower absorption and therefore gives rise to only a small number of overtones.

In the following we will discuss selected regions of the observed Raman spectra of $^{79}Br^{35}Cl$ and show how the spectra can be simulated by two different approaches. First we discuss the overtone spectra of $^{79}Br^{35}Cl$, then the derivation of potential functions. A chapter on time dependent aspects will follow before depolarization ratios will be discussed. The fundamental region will be considered at the end because of special reasons.

4.2 Overtone spectra of $^{79}Br^{35}Cl$ and electronic Raman spectrum of the ^{35}Cl atom.

In panel A of Fig. 3 we display the region of the first overtone of $^{79}Br^{35}Cl$ obtained under high resolution (about 0.7 cm^{-1}) for various excitation wavelengths in the visible region as indicated. Besides the Q branches of $^{79}Br^{35}Cl$ which spread over the spectral region from about 830 to 880 cm^{-1}, a sharp peak can be observed at 882.5 cm^{-1} (labeled by an asterisk). This sharp band represents the electronic transition $^2P_{1/2} \leftarrow {}^2P_{3/2}$ of the chlorine atoms, which are produced through photodissociation of BrCl. Here unimolecular dissociation competes with continuum resonance Raman scattering. As shown the resulting products can also be observed via Raman scattering. In the case of halogen atoms this type of scattering was first observed by Chang *et al*[44,45]. They studied the electronic Raman transitions of atomic chlorine and bromine at 882.5 and 3685 cm^{-1}, respectively. Ganz and Kiefer[46] and Ganz *et al*[47] measured the atomic Raman transition in iodine and partially resolved the hyperfine structure within this electronic Raman transition. Similar results were also obtained for $^{79}Br_2$ and $^{81}Br_2$ [Ref. 47]. The hyperfine splitting in the case of the chlorine atom is too small to be detected by conventional Raman spectroscopy. Nevertheless in Fig. 3, panel A we see an illustrative example of simultaneous observation of continuum resonance Raman and electronic Raman scattering.

The first overtone consists for every exciting wavelengths (Fig. 3, panel A) of four partially resolved Q branches i.e. the fundamental transition Q(1←0) at 877 cm^{-1}, the first hot band Q(3←1) at 870 cm^{-1}, the second hot band Q(4←2) at 862 cm^{-1}, and the third hot band Q(5←3) at 855 cm^{-1}. For excitation with 496.5,

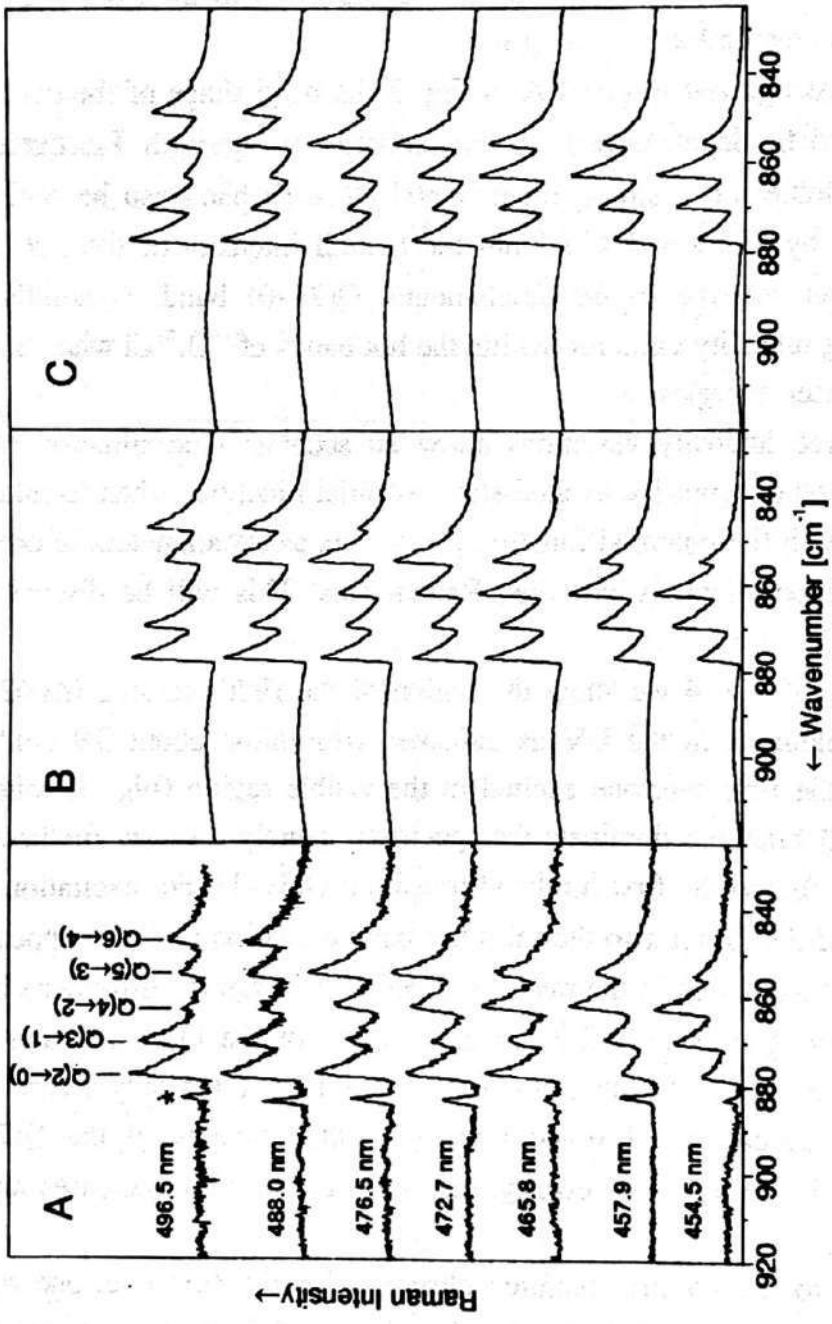

Fig. 3. Continuum resonance Raman spectra of the first overtone region ($\Delta v=2$) of $^{79}Br^{35}Cl$ excited with different argon ion laser lines in the visible region as indicated; panel A: experimentally observed spectra; panel B and C: theoretically calculated spectra applying the KHD- and the time dependent approaches, respectively. The band arising from electronic Raman scattering in the ^{35}Cl atom is marked by an asterisk.

488.0 and 476.5 nm even the fourth hot band Q(6←4) at 848 cm^{-1} is visible. The weak broad bands from about 880 cm^{-1} to 920 cm^{-1} correspond to many unresolved S branch transitions with Δv=2. The O branch transitions have even weaker intensity and appear only as a monotonic background. The electronic transition in ^{35}Cl (labeled by an asterisk) is observed with different intensities depending on the excitation wavelength.

As can be recognized in panel A of Fig. 3 the band shape of the overtones show a characteristic dependence from the excitation wavelength. For excitation from 496.5 to 465.8 nm a strong fundamental Q(2←0) band can be observed. With excitation by 457.9 and 454.5 nm the overall intensity of the hot bands becomes stronger relative to the fundamental Q(2←0) band. Generally, we obverve a strong intensity variation within the hot bands of $^{79}Br^{35}Cl$ when excited with different laser energies.

The sensitive intensity variations allow an accurate determination of the shape and position of repulsive excited-state potential functions when simulations are performed with the potential function parameters as fitparameters in order to reproduce the experimentally observed Raman data. This will be discussed in section 5.3.

In panel A of Fig. 4 we show the region of the first overtone (Δv=2) for excitation wavelengths in the UV as indicated (resolution about 0.9 cm^{-1}). In comparison to the first overtone excited in the visible region (Fig. 3, panel A) here only two Q branches dominate the spectrum, namely a strong fundamental transition Q(2←0) and the first hot band transition Q(3←1). For excitation with 335.8, 334.5 and 333.6 nm also the third hot band transition Q(4←2) appears as a weak shoulder. Although in the range of 335.8 - 333.6 nm the difference in the exciting laser energies is only 2.2 nm an increase of the Q(4←2) band with increasing laser energy is visible. For excitation with 363.8 nm only a very weak hot band Q(3←1) can be observed relative to the intensity of the Q(2←0) transition. With increasing laser energy, the Q(3←1) transition increases rapidly in intensity.

Compared to the spectral features observed for the first overtone region where a monotonic change of the hot band intensities is found (Fig. 4, panel A), the changes for excitations in the visible region are more pronounced (Fig. 3, panel A).

Fig. 5, panel A displays the third overtone. The intensities for the hot band transitions increase with increasing laser energy similar to the observations for the second overtone excited in the UV region (Fig. 4, panel A).

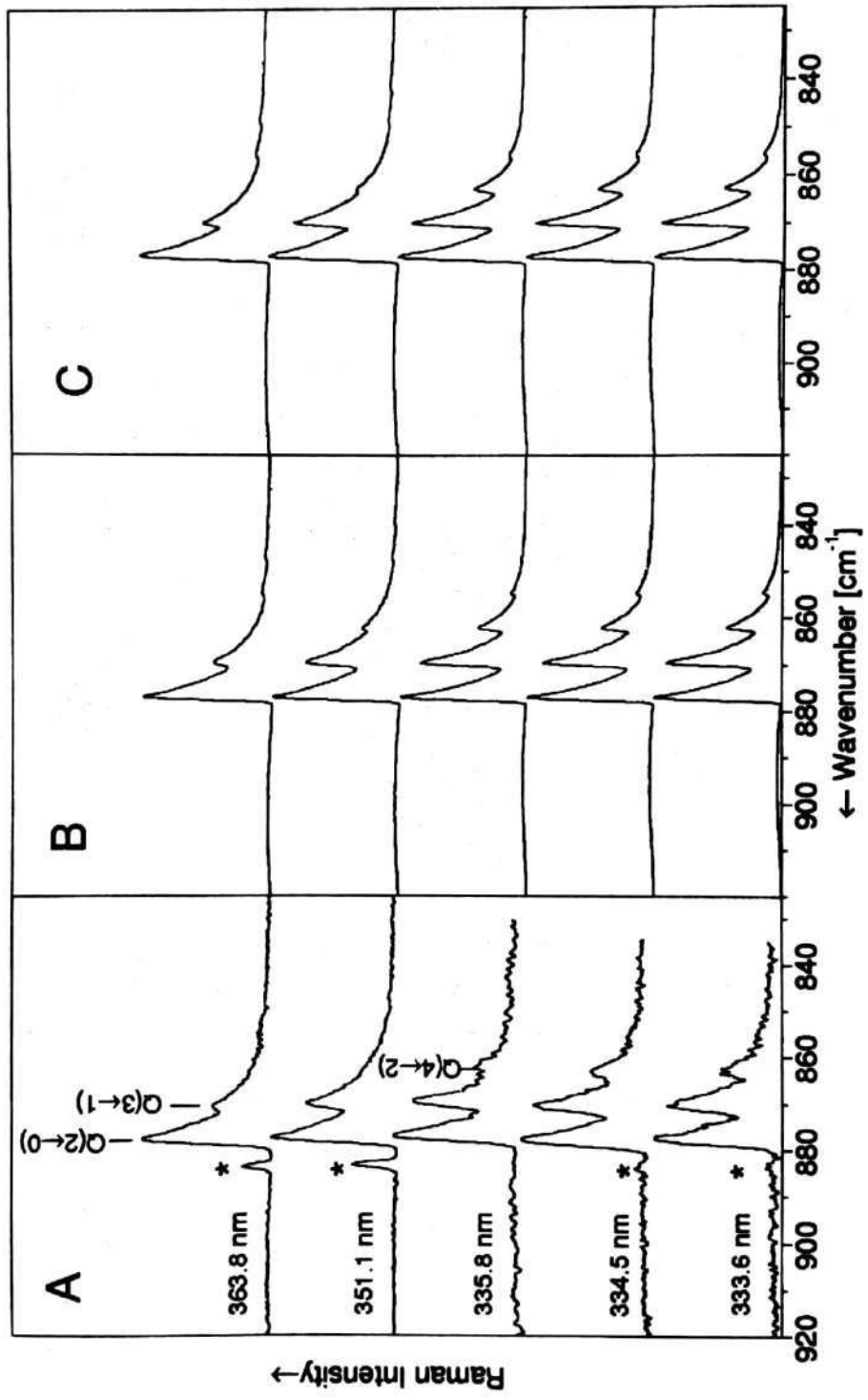

Fig. 4. Same as Fig. 3 except for excitation with argon ion laser lines in the UV region as indicated.

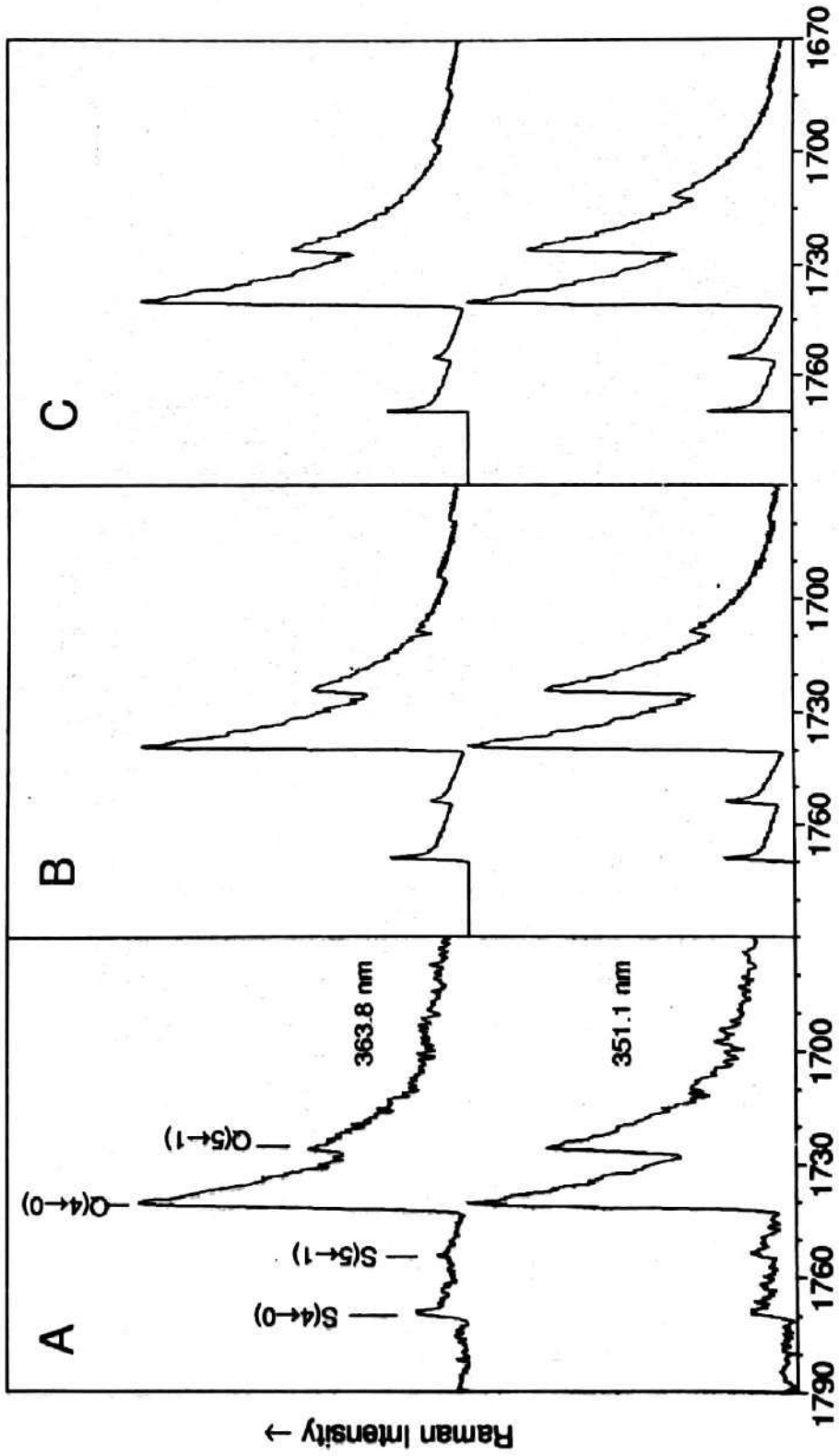

Fig. 5. Same as Figure 3 except for the third overtone region ($\Delta v=4$) and excitation with the two argon ion laser lines at 363.8 and 351.1 nm.

We notice that for higher changes in the vibrational quantum number (Δv) the intensity distribution within an overtone region does not change dramatically. This is similar to the situation in $^{127}I^{35}Cl$ [Ref. 9] but differs from what has been observed in $^{127}I^{79}Br$ [Ref. 10]. In the case of $^{127}I^{79}Br$ the overtones showed large variations in the intensity patterns.

In the third overtone (Fig. 5, panel A) additional sharp S band heads can be observed on the higher energy side of the Q branches. Such S band heads are the predominant features in the spectra of higher overtones. As has been demonstrated[48,49] S band heads are to be observed when the J value which corresponds to the band head ($J_{max}(\Delta v)$) is close to the J value for maximum vibrational-rotational Raman intensity ($J_{max}(T)$), which means that $|\,(J_{max}(\Delta v) - (J_{max}(T))\,|$ is small.

4.3 Determination of excited state potential functions from resonance Raman spectra

As known, the intensity of a vibrational transition in continuum resonance Raman scattering depends strongly on the excitation energy[8,15,18,19]. In the case that more than one excited state contributes to the scattering intensity, the result is not simply the numerical sum of the specific contributions of the single states. According to Eq. (6) of Ref. [21] there is also destructive or constructive interference between the excited states depending on the signs of the real and imaginary parts of the functions χ_B and χ_Π (third term of Eq. (6)). Thus theoretical simulations of continuum resonance Raman spectra with the inclusion of scattering from both states allow us to derive information of the excited state potential functions with high accuracy.

In Figs. 6 and 7 we show the experimentally observed (A) continuum resonance Raman spectra of the first overtone ($\Delta v=2$) of the $^{79}Br^{35}Cl$ molecule for one wavelength in the visible and one in the UV region (457.9 and 363.8 nm, respectively) and compare them with numerically calculated spectra by making use of the conventional (KHD) theory (left panel) and the time dependent theory (right panel). The spectra labeled by (B) are the results of calculations where two states, $B(^3\Pi_{0+})$ and $^1\Pi_1$, have been taken as contributing excited electronic states (all three terms in Eq. (6) of Ref. [21]), whereas in panels C and D the contributions of the single states (only term one and term two of Eq. (6) of Ref. [21], respectively) are plotted. The theoretical spectra were calculated applying Eq. (5) and (9) of Ref. [21] for the KHD and time-dependent approach,

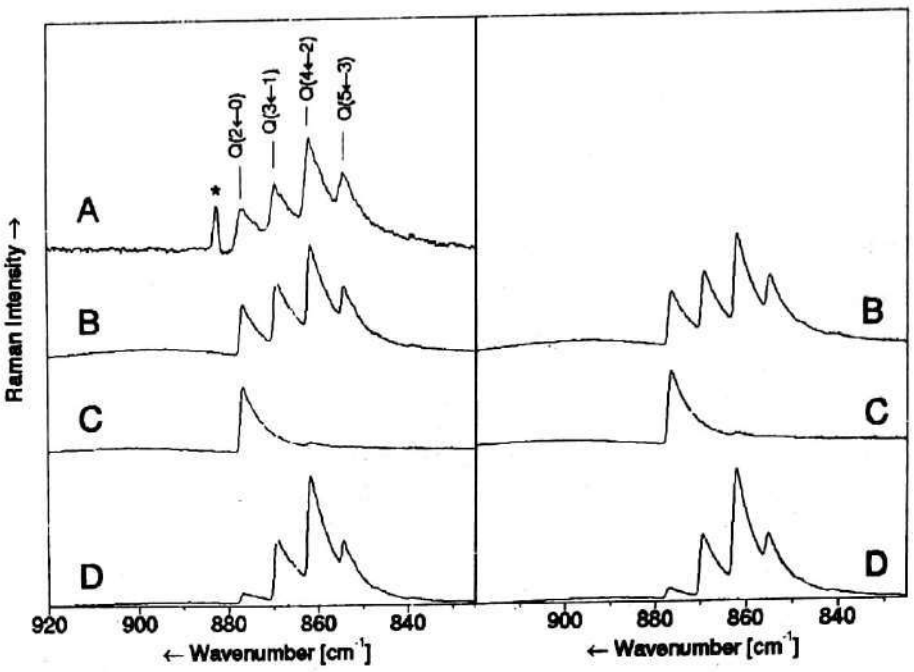

Fig. 6. Continuum resonance Raman spectra of the first overtone transition ($\Delta v=2$) of $^{79}Br^{35}Cl$ with $\lambda_0=457.9$ nm excitation. Left panel: (A) experimentally observed spectrum (same as Figure 3); (B) calculated spectrum applying the conventional (KHD) approach with inclusion of two excited electronic states ($B(^3\Pi_{0+})$ and $^1\Pi_1$ state). Spectra (C) and (D) represent contributions from the continuum of the $^3\Pi_{0+}$ or $^1\Pi_1$ state alone, respectively. Right panel: spectra (B)-(D) same as in left panel except for time dependent theory. For asterisk see Fig. 3.

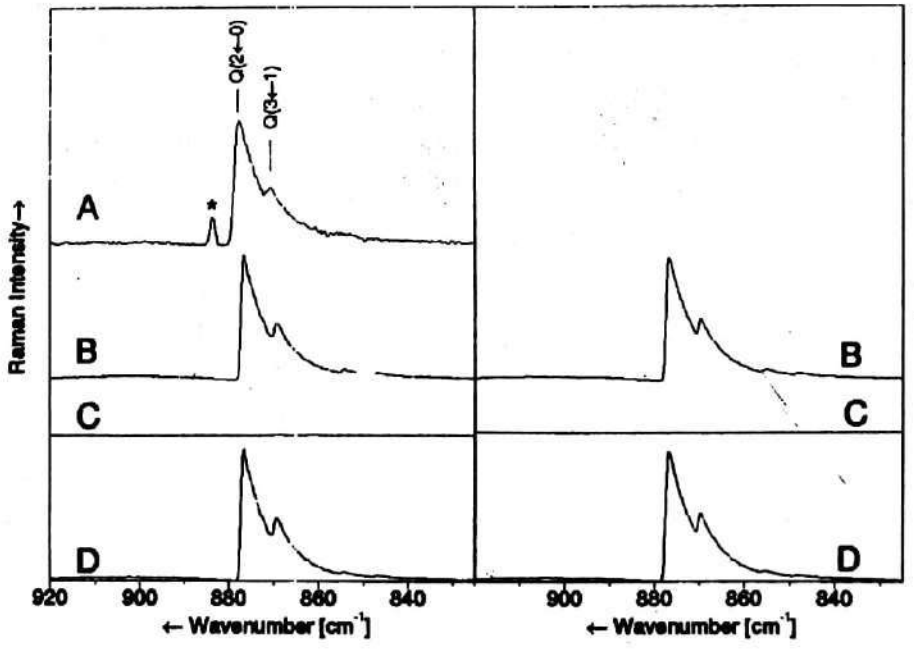

Fig. 7. Same as Fig. 6 except for $\lambda_0=363.8$ nm.

respectively. The position and form of the excited state potential functions were varied in order to achieve best agreement between measured and calculated spectra.

The calculations show that for 457.9 nm excitation both potentials contribute to the scattering process (see Fig. 6). The hot band transitions Q(3←1), Q(4←2) and Q(5←3) originate only from scattering via the Π state (panel D) whereas the fundamental band (Q(2←0)) arises mainly from $^3\Pi_{0+}$ scattering (panel C). The agreement between calculated (panel B) and experimentally obtained spectra (panel A) is good. Note that in the calculated spectra the electronic transition in ^{35}Cl (asterisk in the experimental spectrum) has not been considered.

For excitation in the UV region at 363,8 nm (see Fig. 7) the vibrational-rotational structure is quite different from that in the visible region. Here the spectrum is determined by a strong fundamental (Q(2←0)) band and only a weak first hot band. The calculations reveal that the total spectrum originates from scattering only via the $^1\Pi_1$ state. There is no contribution of the B state as revealed from panels C.

As outlined above, excitation of $^{79}Br^{35}Cl$ in the visible region is via two interacting excited electronic states. To what extent the specific excited states contribute to the continuum resonance Raman scattering intensity is determined by the electronic transition moments, M_e, as well as by the values of the Franck Condon factors of the vibrational transitions. Because we are dealing here with relative intensities, we cannot determine the absolute values of the electronic transition moments, but only the ratio $\Re = M_B/M_\Pi$. The electronic transition moments for BrCl are not known. Therefore we took the ratio of the electronic transition moments, and the shape and position of the $^3\Pi_{0+}$ and $^1\Pi_1$ states as fit parameters for the simulation of the observed resonance Raman spectra in the visible region.

In panel A of Fig. 3 we have displayed the experimental spectra of the first overtone ($\Delta v=2$), excited with seven argon ion laser lines in the visible region (496.5, 488.0, 476.5, 472.7, 465.8, 457.0 and 454.5 nm) together with the KHD (panel B) and time dependent (panel C) calculations. For these simulations the optimized potential data as given in table 1 were used.

In summary both simulations agree fairly well with the experiment, although remarkable intensity changes of the fundamental and hot band transitions occur for excitation with the various laser lines.

Similar good results were obtained for the spectra excited with UV argon ion laser lines (see Figs. 3 and 4). For these calculations we have considered only

contributions from the $^1\Pi_1$ state potential curve.

Table 1--Potential parameters for the repulsive parts of the excited states $B(^3\Pi_{0+})$ and $\Pi(^1\Pi_1)$ of $^{79}Br^{35}Cl$ as derived from the optimized simulations of experimentally observed continuum resonance Raman spectra.

State e	M_B/M_Π	C (cm^{-1})	γ (nm^{-1})	r_e(nm)	V_e(cm^{-1})
$^1\Pi_1$	1.0	8200±170	49.87±1	0.2144 ±0.0004	18244
$^3\Pi_{0+}$	0.7±0.07	5240±170	73.37±3	0.2444 ±0.0002	18479

4.5 Time dependent aspects

The time dependent approach to simulate the continuum resonance Raman spectra opens up a new insight in the scattering process. To understand and to analyze the interesting time evolution of Raman spectra it is helpful to plot the time dependent Franck-Condon overlap functions and the modulus of their integrals as a function of time. The modulus of the time dependent overlap functions of $^{79}Br^{35}Cl$ differs not in its common behaviour from those obtained for $^{127}I^{35}Cl$ [Ref. 21] or $^{127}I^{79}Br$ [Ref. 33]. Only the positions of the maxima and minima shift by a few femtoseconds on the time scale. Therefore we have not diplayed here these functions and refer to Refs. [21,22,33]. We also found, that the reflection principle discovered by Kolba *et al*[50] is valid for $^{79}Br^{35}Cl$.

It is also of interest to plot the modulus of the integral over the time dependent Franck-Condon factors as a function of time. These values do not increase monotonically with time, instead they show distinct maxima. The latter are caused by the oscillatory behaviour of real and imaginary part of the overlap integrals. The integration over time can lead to smaller intensity values at later times. This effect can be interpreted as destructive interference of contributions from different time intervals during the propagation of the wave packet. A very nice example demonstrating this effect is the fundamental Q(2←0) transition in $^{79}Br^{35}Cl$ calculated with contribution of only the $^1\Pi_1$ state and excited with 457.9 nm. The corresponding modulus of the integral over the time dependent Franck-Condon factors as a function of time is shown in Fig. 8. Note that the final modulus has much lower value after some ten femtoseconds, since a maximum

at about 6 fs is formed. Such a high value for the maximum has not yet been observed before.

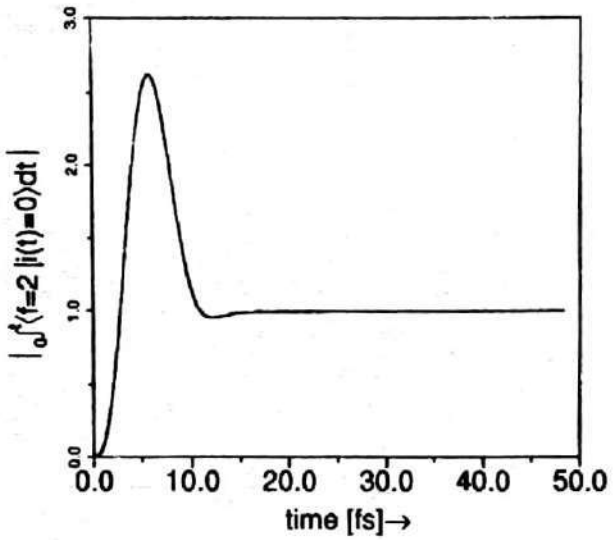

Fig. 8. Absolute values of the time-integrated overlaps for the Stokes transition for continuum resonance Raman scattering in $^{79}Br^{35}Cl$ from the initial vibrational state $|i=0\rangle$ to the final state $|f=2\rangle$ and excitation with λ_0=457.9 nm as a function of time. For this calculation only the$B(^3\Pi_{0^+})$ state was taken into account.

The time dependent approach allows also to derive scattering delay times, i.e. the time which passes between excitation and deexcitation to and from the excited electronic states, respectively. This delay time corresponds to the average propagation time of the wave packet until the molecule returns to his electronic ground state. The definition for the scattering delay time t_{fi} and further details are given in Ref. [21] and References therein. The calculated scattering delay times for $^{79}Br^{35}Cl$ are between 7 and 20 fs. Comparing corresponding transitions in bromine chloride with those in iodine chloride or iodine bromide, we find that the t_{fi} values are lower than the values for the two other interhalogen molecules.

4.6 The fundamental Raman band

Until now we have not discussed the spectra of the fundamental region in $^{79}Br^{35}Cl$. The experimental observations of this fundamental region gives us reasons to discuss it separately. First, we display in Fig. 9 the spectra of the fundamental region excited with 12 different laser lines from 514.5 nm - 335.8 nm measured with a resolution smaller than appr. 1 cm^{-1}. All spectra show a strong intensity variation within the fundamental and hot band transitions. A qualitative investigation of the Q bands leads to an interesting conclusion. In the

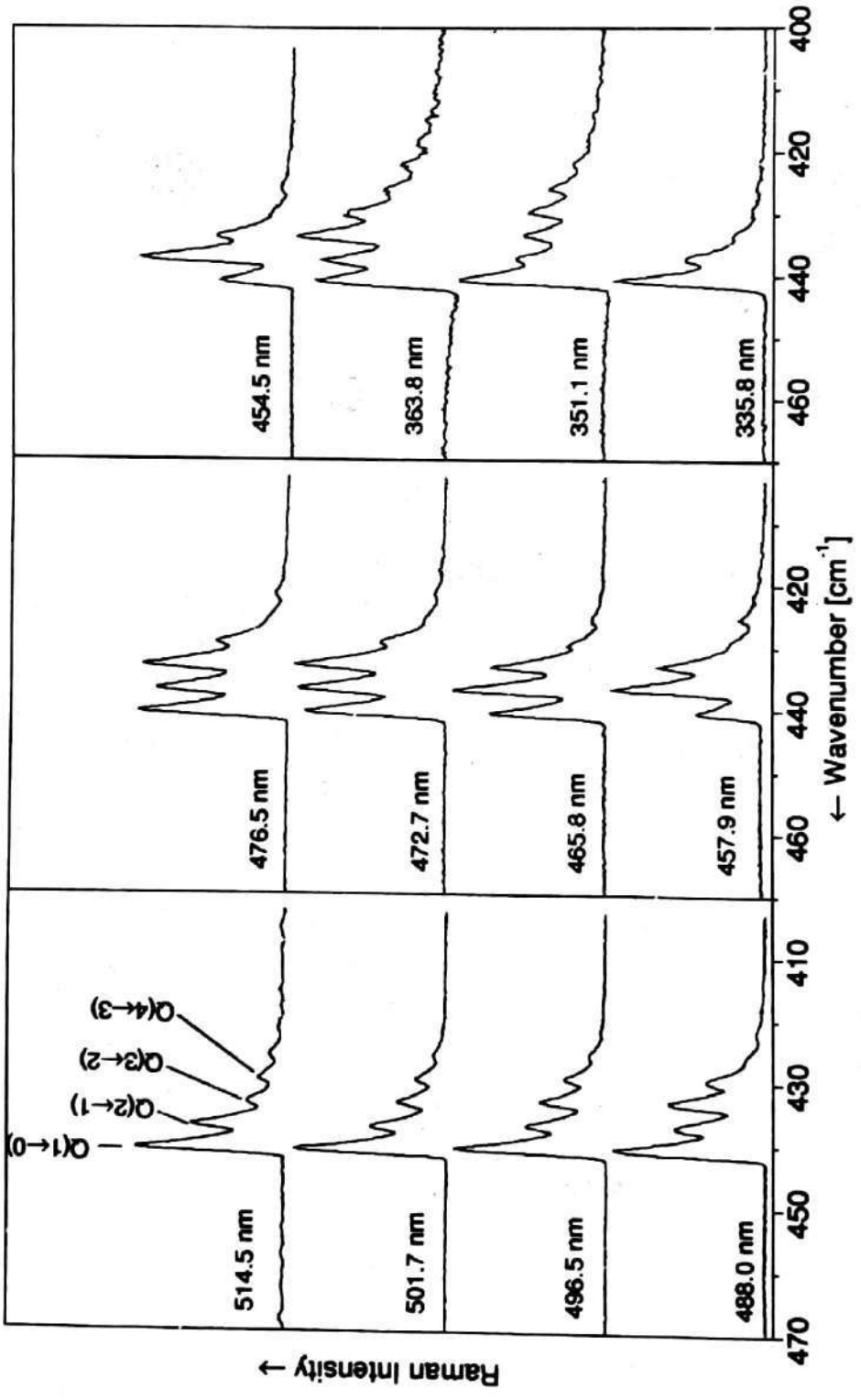

Fig. 9. Experimentally observed Raman spectra of the fundamental region ($\Delta v=1$) excited with various argon ion laser lines as indicated.

visible region (514.5-454.5 nm) the intensities of the hot bands grow up with increasing laser energy (e.g. the Q(3←2) or the Q(4←3) relative to the intensity of the fundamental Q(1←0)), whereas in the UV region (363.8-333.6) the intensities of these hot bands decrease with increasing laser energy. Assuming pure continuum resonance Raman scattering and with the potential parameters in table 1 we could not simulate these spectra. As in former experimental works[4,6] we obtain for all exciting laser wavelengths a high intensity for the fundamental region compared to the intensities of the corresponding overtone transitions except for the excitation with 363.8 and 351.1 nm. In table 2 the intensities of the fundamental region for various exciting laser lines from the visible to the UV region normalized to the first overtone are listed. The error in the determination of the experimental overall intensities is about 10%.

Table 2--Observed Raman intensities of the fundamental band and overtones of $^{79}Br^{35}Cl$ normalized to the first overtone ($\Delta v=2$) excited with various laser lines from the visible to the UV region.

	Vibrational transition				
Excitation wavelength	$\Delta v=1$	$\Delta v=2$	$\Delta v=3$	$\Delta v=4$	$\Delta v=6$
472.6 nm	12.23	1.00	---	---	---
457.9 nm	4.44	1.00	---	---	---
363.8 nm	1.54	1.00	0.55	0.39	0.18
351.1 nm	1.74	1.00	0.51	0.31	0.18
335.8 nm	6.88	1.00	0.65	---	---
333.6 nm	8.47	1.00	0.67	---	---

In table 3 the corresponding calculations assuming pure continuum resonance Raman scattering are shown. One can observe that the experimental intensity ratios within the overtone transitions agree fairly well with the calculated values. But in the case of the fundamental region ($\Delta v=1$) strong deviations occur. An analogous situation was found by Strempel and Kiefer for $^{35}Cl_2$ [Ref. 8].

Table 3--Calculated Raman intensities of the fundamental band and overtones of $^{79}Br^{35}Cl$ relative to the first overtone ($\Delta v=2$) excited with various laser lines from the visible to the UV region and assuming pure continuum resonance Raman scattering.

	Vibrational transition				
Excitation wavelength	$\Delta v=1$	$\Delta v=2$	$\Delta v=3$	$\Delta v=4$	$\Delta v=6$
472.6 nm	2.43	1.00	---	---	---
457.9 nm	1.83	1.00	---	---	---
363.8 nm	2.50	1.00	0.54	0.36	0.18
351.1 nm	2.53	1.00	0.53	0.36	0.22
335.8 nm	2.59	1.00	0.53	---	---
333.6 nm	2.63	1.00	0.55	---	---

Considering the absorption spectra of both molecules in Fig. 2 one can also see an nearly identical structure. In both spectra the maximum corresponds to the repulsive $^1\Pi_1$ state. The contribution of the bounded $^3\Pi_{0+}$ is visible in both absorption spectra as a shoulder on the low energy side. The shoulder in $^{35}Cl_2$ is much weaker than in $^{79}Br^{35}Cl$, visible also in different wavelength dependent contributions of the $^3\Pi_{0+}$ state to the scattering process. For details concerning the scattering in $^{35}Cl_2$ see Ref. [8]. Therefore the reasons for the high scattering intensity of the fundamental region are the same as for $^{35}Cl_2$, which means that there exists besides continuum resonance Raman scattering normal nonresonant scattering via high lying excited electronic states. In the case of high absorption (363. 8 or 351.1 nm) and thus enhancement of the Raman scattering due to the common resonance effect the detected small intensities (even smaller than the calculated value assuming pure continuum resonance Raman scattering) are caused by destructive inference between resonant and nonresonant scattering. A further proof for this statement can be made through depolarization ratio measurements for different exciting wavelenghts. This will be discussed next.

4.7 Depolarization ratios

In table 4 we have displayed the measured depolarization ratios for the Q(1←0) transition excited with various wavelengths.

Table 4--Depolarization ratios for the fundamental band ($\Delta v=1$) for $^{79}Br^{35}Cl$ excited with different wavelengths as indicated

Excitation wavelength / nm	$\rho(Q_{1\leftarrow 0})$
514.5	0.0054±0.05
501.7	0.0057±0.05
496.5	0.058±0.005
488.0	0.059±0.005
476.5	0.048±0.005
472.7	0.057±0.005
465.8	0.042±0.005
457.9	0.030±0.005
454.5	0.020±0.005
363.8	0.269±0.015
351.1	0.109±0.015
334.5	0.055±0.015

As mentioned above, in the visible region both the $^3\Pi_{0+}$ and the $^1\Pi_1$ state contribute to the scattering process. Scattering via only the $^3\Pi_{0+}$ state would result in a depolarization ratio of 0.125, scattering via the $^1\Pi_1$ state results in a value of 0.04 [Ref. 16]. From our experiences in $^{127}I^{35}Cl$ [Refs. 20,21] and $^{127}I^{79}Br$ [Ref. 22] scattering via two states leads to strong wavelength dependent variations of the depolarization ratios. In the case of $^{79}Br^{35}Cl$ we observe a nearly constant depolarization ratio (about 0.05) in the visible region. Furthermore in the UV region, where the $^1\Pi_1$ state plays the exclusively dominant role, one would expect in the case of pure continuum resonance Raman scattering a value for the depolarization ratio of 0.04. Instead of this we obtain high values in the case of strong absorption (351.1 nm) and again the same constant value (about 0.05) in the case of relative weak absorption (334.5 nm). Summarizing these results, we can conclude, that the scattering process for the fundamental region of $^{79}Br^{35}Cl$ is mainly dominated by nonresonant scattering over unknown highly lying adjacent states. Only in the case of a strong resonance Raman effect (region of high

absorption) the scattering occurs by pure resonant Raman scattering resulting in destructive interference of the scattering intensity and remarkable changes of the depolarization ratios.

In table 5 we add the results obtained for the depolarization ρ of the Q(2←0) Raman transition for three different wavelengths in the UV region.

Table 5--Observed and calculated depolarization ratios of the Q branches for the Q(2←0) transition (Δv=2) of $^{79}Br^{35}Cl$ as a function of the excitation wavelength.

Excitation wavelength	Depolarization ratio ρ for the Q(2←0) band	
(nm)	observed	calculated
363.8	0.05±0.015	0.04
351.1	0.06±0.015	0.04
334.5	0.08±0.015	0.04

From the values obtained we can draw the conclusion that the scattering process for excitation in the UV region involves exclusively an Ω=1 state. This nicely supports the results derived from the simulations of the observed spectra as discussed above.

5 Conclusion

We have presented experimentally and numerically simulated continuum resonance Raman spectra of isotopically pure $^{79}Br^{35}Cl$ applying conventional and time-independent quantum theory. Good agreement between experimentally observed and calculated spectra could be obtained for various excitation laser lines from the visible to the UV region. We found that in bromine chloride there are two excited state potentials which contribute to the scattering process for excitation in the visible region, i.e. the $^3\Pi_{0+}$ and the $^1\Pi_1$ state. Compared to other interhalogen molecules like $^{127}I^{35}Cl$ and $^{127}I^{79}Br$ the contribution of the $^3\Pi_{0+}$ is the lowest. In the UV region the $^1\Pi_1$ state exclusively dominates the scattering process. The parameters for the excited state potential functions could be obtained with fairly high accuracy. The scattering process for the fundamental region of $^{79}Br^{35}Cl$ is mainly dominated by nonresonant scattering via hitherto unknown highly lying electronic states. Only in the case of strong resonance Raman effect the scattering is influenced by pure continuum resonance Raman scattering. This

phenomenon is similar to the one earlier found for $^{35}Cl_2$ and is visible in destructive interference of the resonant and nonresonant scattering intensities and remarkable changes of the depolarization ratios.

Acknowledgements

We highly acknowledge financial support from the Deutsche Forschungsgemeinschaft (Sonderforschungsbereich 347, Teilprojekt C2) as well as from the Fonds der Chemischen Industrie. We also thank Dr. M. Ganz for many helpful discussions.

References

1 Stammreich H & Forneris R, *J Chem Phys*, 21 (1953) 944.
2 Wallart F, *Can J Spectrosc*, 17 (1972) 128.
3 Wight C A, Ault B S & Andrews L, *J Mol Spectrosc*, 56 (1975) 239.
4 Holzer W, Murphy W F & Berstein H J, *J Chem Phys*, 52 (1970) 399.
5 Chang H, Wang J L & Tzeng G D, *J Chin Chem Soc (Tapei)*, 33(1) (1986) 1.
6 Chang H & Lin H M, *Proc Natl Sci Counc B, ROC* 5 (1981) 263.
7 Chang H, Tien S G & Hwang M H, *Proc Natl Sci Counc B, ROC*, 7 (1983) 420.
8 Strempel J & Kiefer W, *J Chem Phys*, 95 (1991) 2391.
9 Ganz M & Kiefer W, *Asian J Physics*, 3 (1992) 111.
10 Vogt P, Deckert V & Kiefer W, *J Raman Spectrosc*, 23 (1992) 365
11 Kramers H A & Heisenberg W, *Z Physik*, 23 (1925) 681.
12 Dirac P A M, *Proc Roy Soc*, A114 (1927) 710.
13 Rousseau D L & Williams P F, *J Chem Phys*, 64 (1976) 3519.
14 Baierl P & Kiefer W, *J Raman Spectrosc*, 10 (1981) 197.
15 Baierl P & Kiefer W, *J Raman Spectrosc*, 11 (1981) 393.
16 Baierl P & Kiefer W, *J Raman Spectrosc*, 10 (1984) 360.
17 Baierl P, Kiefer W, Williams P F & Rousseau D L, *Chem Phys Lett*, 50 (1977) 57.
18 Strempel J & Kiefer W, *J Raman Spectrosc*, 22 (1991) 583.
19 Strempel J & Kiefer W, *Can J Chem*, 69 (1991) 1732.
20 Ganz M, Strempel J & Kiefer W, *Chem Phys Lett*, 207 (1993) 110.
21 Ganz M & Kiefer W, *Mol Phys*, 81 (1994) 69.
22 Vogt P & Kiefer W, *J Raman Spectrosc*, in press.
23 Hizhnyakov V & Tehver I J, *Phys stat sol*, 21 (1967) 755.
24 Lee S Y & Heller E J, *J Chem Phys*, 71 (1979) 4777.
25 Heller E J, *Acc Chem Rep*, 14 (1981) 368.
26 Tannor D J & Heller E J, *J Chem Phys*, 77 (1982) 202.
27 Williams S O & Imre D G, *J Phys Chem*, 92 (1968) 3368.

28 Kosloff R, *J Phys Chem*, 92 (1988) 2087 and references cited therein.
29 Hartke B, *Chem Phys Lett*, 160 (1989) 538.
30 Hartke B, *J Raman Spectrosc*, 22 (1991) 131.
31 Hartke B, Kiefer W, Kolba E, Manz J & Strempel J, *J Chem Phys*, 96 (1992) 5636.
32 Ganz M & Kiefer W, *J Raman Spectrosc*, 24 (1993) 463.
33 Vogt P, Schmitt M & Kiefer W, *Chem Phys Lett*, 243 (1995) 64.
34 Vogt P, Schmitt M & Kiefer W, *J Raman Spectrosc*, 26 (1995) 861.
35 Deckert V & Kiefer W, *Appl Spectrosc*, 46 (1992) 322.
36 Rydberg R, *Z Physik*, 73 (1931) 376.
37 Klein O, *Z Physik*, 76 (1932) 226.
38 Rees A L G, *Proc Phys Soc*, London A59 (1942) 998.
39 Coxon J A, *J Mol Spectrosc*, 50 (1974) 142.
40 Mc Feeters B D, Perram G P, Crannage R P & Dorko E A, *Chemical Physics*, 139 (1989) 347.
41 Weast R C & Lide D R, *Handbook of Chemistry and Physics* (1990) CRC Press, Inc, USA.
42 Seery D & Britton D, *J Phys Chem*, 68 (1964) 2263.
43 Kiefer W, Ganz M, Vogt P & Schmitt M, *J Mol Struct*, 347 (1995) 229.
44 Chang H, Lin H M & Hwang M H, *J Raman Spectrosc*, 15 (1984) 205.
45 Chang H & Chen S H, *J Raman Spectrosc*, 17 (1986) 453.
46 Ganz M & Kiefer W, *Chem Phys Lett*, 188 (1992) 395.
47 Ganz M, Vogt P, Deckert V & Kiefer W, *Phys Lett*, A187 (1994) 317.
48 Kiefer W & Bernstein H J, 43 (1972) 366.
49 Baierl P & Kiefer W, *J Raman Spectrosc*, 3 (1983) 353.
50 Kolba E, Manz J, Schreier H J & Trisca I, *Chem Phys Lett*, 189 (1992) 505.

[*Received* 1 1 96; *accepted* 28 1 96]